Matter and Radiation at Extremes

RESEARCH ARTICLE

pubs.aip.org/aip/mre

Pressure-induced evolution of stoichiometries and electronic structures of host–guest Na–B compounds

Cite as: Matter Radiat. Extremes 8, 068401 (2023); doi: 10.1063/5.0155005
Submitted: 17 April 2023 • Accepted: 27 August 2023 •
Published Online: 19 September 2023

Zixuan Guo,[1] Xing Li,[1] Aitor Bergara,[2,3,4] Shicong Ding,[1] Xiaohua Zhang,[1] and Guochun Yang[1,a)]

AFFILIATIONS

[1] State Key Laboratory of Metastable Materials Science & Technology and Key Laboratory for Microstructural Material Physics of Hebei Province, School of Science, Yanshan University, Qinhuangdao 066004, China
[2] Departamento de Física and EHU-Quantum Center, Universidad del País Vasco-Euskal Herriko Unibertsitatea, UPV/EHU, 48080 Bilbao, Spain
[3] Donostia International Physics Center (DIPC), 20018 Donostia, Spain
[4] Centro de Física de Materiales CFM, Centro Mixto CSIC-UPV/EHU, 20018 Donostia, Spain

Note: Paper published as part of the Special Topic on High Pressure Science 2023.
[a)] **Author to whom correspondence should be addressed:** yanggc468@nenu.edu.cn

ABSTRACT

Superionic and electride behaviors in materials, which induce a variety of exotic physical properties of ions and electrons, are of great importance both in fundamental research and for practical applications. However, their coexistence in hot alkali-metal borides has not been observed. In this work, we apply first-principles structure search calculations to identify eight Na–B compounds with host–guest structures, which exhibit a wide range of building blocks and interesting properties linked to the Na/B composition. Among the known borides, Na-rich Na_9B stands out as the composition with the highest alkali-metal content, featuring vertex- and face-sharing BNa_{16} polyhedra. Notably, it exhibits electride characteristics and transforms into a superionic electride at 200 GPa and 2000 K, displaying unusual Na atomic diffusion behavior attributed to the modulation of the interstitial anion electrons. It demonstrates semiconductor behavior in the solid state, and metallic properties associated with Na $3p/3s$ states in the superionic and liquid regions. On the other hand, B-rich NaB_7, consisting of a unique covalent B framework, is predicted to exhibit low-frequency phonon-mediated superconductivity with a T_c of 16.8 K at 55 GPa. Our work advances the understanding of the structures and properties of alkali-metal borides.

I. INTRODUCTION

Alkali metals, with the simplest single-valence-electron configuration and remarkably high chemical reactivity, have long been considered as a paradigm in fundamental physics, especially in the development of the electronic theory of solids.[1] Under ambient conditions, all alkali metals form a body-centered cubic lattice and exhibit intrinsic metallicity.[2–4] However, under high pressure, they undergo complex structural phase transitions, accompanied by exotic electron behaviors, such as $s \rightarrow p/d$ charge transfer[5,6] and valence electrons located in lattice interstitials and acting as anionic electrons (i.e., electrides[7]), as well as interesting electronic properties, including metal–semiconductor/insulator transitions,[7–9] superconductivity induced by interstitial electrons,[10] and so on. Thus, alkali metals remain an important and active topic in the field of high-pressure physics.[11–16]

On the other hand, alkali metals have the ability to form unconventional compounds, especially at high pressures, and this has played an increasingly important role in fundamental research.[17–22] For instance, at high pressure, Na can react with He atoms, which are chemically very inert, resulting in the first thermodynamically stable compound Na_2He with an electride character, which can be attributed to the eight-center two-electron bonds of the empty Na_8 cubes.[19] Recently, pressure-induced Li-rich Li–Al compounds have also been found to be electrides, in which Al atoms exhibit diverse oxidation states owing to differences in Li → Al charge transfer.

Even more interestingly, the Li_6Al electride, with two-dimensional sheets of Li composed of five- and eight-membered rings, exhibits an unexpected coexistence of superconductivity and superionicity.[20] Consequently, alkali metals have unique advantages in triggering novel physical and chemical properties.[23]

Alkali-metal borides with B-rich stoichiometry, stabilized at high pressures, have also attracted great interest, because the weak ionic interaction between alkali metals and B units facilitates the stabilization of new B allotropes, and the electrons donated by alkali metals can compensate for the electron deficiency of B atoms.[24–26] This type of study has not only promoted the discovery of materials with interesting properties (e.g., hardness[27] and superconductivity[24]), but has also become a routine way to access new B allotropes. Our group proposed two hitherto unknown B allotropes (B_4 and B_{17}) with the highest superconducting transition temperature among bulk boron allotropes at that time, which were successfully obtained by removing the Na atoms from the predicted high-pressure phases of NaB_4 and Na_2B_{17}.[24,28] In the K/Rb–B system, the metastable KB_4 and the stable RbB_8 compounds were theoretically identified and considered as ideal precursors to obtain a two-dimensional B sheet (a double layer consisting of six-membered rings) and the bulk o-B_{16} phase in an experimental synthesis.[25,26] On the other hand, Ma and co-workers[29] proposed the idea of designing Li-rich borides (Li_xB, x = 1, 1.5, 2, 2.5, 3, . . ., 8) and identified the Li_6B compound, in which B atoms have a full-shell electronic configuration and there are no electrons located in the interstitial regions.

The superionic state, as an intermediate between the solid and liquid states in which some atoms still vibrate around their equilibrium positions while the others can diffuse in certain ways, has broad application prospects in solid-state batteries.[30] Electrides, characterized by the presence of electrons residing at interstitial regions, have also shown unusual properties (e.g., ultra-low work function,[31] high catalytic activity,[32] and superconductivity[33–35]). In addition, interstitial electrons can also mediate superionic behavior.[36] However, superionic electrides are still rather rare. Considering that superionicity usually appears in compounds with weak bonds or light elements, alkali-metal-rich borides have an inherent potential to exhibit coexisting superionic and electride behaviors.

Sodium, with unusual chemical attributes and relatively light mass, has demonstrated a strong ability to stabilize many allotropes and compounds (e.g., $NaSi_6$[37] and Na_6Au[38]) under different conditions. Therefore, we have wondered if modulation of the Na/B ratio combined with pressure could achieve the objective mentioned above. In this work, we perform an extensive first-principles structural search of Na/B-rich Na–B compounds at 100, 200, and 300 GPa, and identify eight previously unknown Na–B compounds with diverse electronic properties, including semiconductivity, metallicity, and superconductivity. Unexpectedly, we find that the Na-richest Na_9B compound is an electride that also exhibits superionic properties at 200 GPa and 2000 K.

II. COMPUTATIONAL METHOD

The intelligence-based particle-swarm optimization algorithm, implemented in the CALYPSO code,[39,40] has become an effective way to predict stable or metastable elemental solids and binary and ternary compounds,[18,41–44] some of which have already been synthesized,[45–49] thereby accelerating the discovery of new materials. Here, we also employed this algorithm to explore the low-enthalpy Na_xB_y phases (x = 1, y = 1, 2, . . ., 20; x = 2, y = 1, 3, 5, . . ., 19; x = 3, y = 1, 2, 20; x = 4, 5, . . ., 12, y = 1) at 100, 200, and 300 GPa. The calculations of structural relaxations and electronic properties were performed with the Vienna *Ab Initio* Simulation Package (VASP).[50] The projector augmented wave (PAW)[51] method was adopted, with $2p^6 3s^1$ and $2s^2 2p^1$ as valence electrons for Na and B atoms, respectively. The Perdew–Burke–Ernzerhof (PBE)[52] generalized gradient approximation was used as the exchange-correlation potential. The validity of the pseudopotentials has been confirmed by the perfect fit of the Birch–Murnaghan equation of states with the full-potential linearized augmented-plane-wave (LAPW) method (Fig. S0, supplementary material).[53] A plane-wave cutoff energy of 850 eV and a Monkhorst–Pack[54] scheme with a k-point grid of $2\pi \times 0.03$ Å^{-1} were adopted to obtain a well-converged enthalpy. Phonon calculations were performed using the supercell finite displacement method in the PHONOPY code.[55] Electron–phonon coupling (EPC) calculations were conducted within density functional perturbation theory (DFPT),[56] as carried out in the QUANTUM ESPRESSO package.[57] *Ab initio* molecular dynamics (AIMD) *NVT* simulations using a 2 × 2 × 1 supercell (160 atoms) for *Imma* Na_9B at 200 GPa were performed for 10 000 steps with a step size of 1 ps at given temperatures of T = 500, 1000, 2000, and 3000 K with the Nosé–Hoover thermostat,[58] and data of the last 2 ps were extracted.

III. RESULTS AND DISCUSSION

A. Phase stability

Inspired by recently reported pressure-induced unconventional stoichiometric compounds (e.g., Li_6Al[20] and CeH_{18}[59]), we have carried out an extensive structure search with 42 stoichiometries of Na_xB_y with up to four formula units per simulation cell to find new Na–B compounds at the selected pressures of 100, 200, and 300 GPa. Based on the identified structures, the energetic stability of the Na_xB_y system [Fig. 1(a)] can be verified by calculating their formation enthalpies relative to the known Na/B elemental solids according to the formula

$$\Delta H(Na_xB_y) = \frac{H(Na_xB_y) - xH(Na) - yH(B)}{x + y}.$$

Generally, the phases that fall on the solid lines of the convex hull in Fig. 1(a) are considered thermodynamically stable, and they do not decompose into elemental solids or other binary compounds, while those on the dashed lines of the convex hull are thermodynamically metastable or unstable, depending on the values of the decomposition enthalpy and the dynamic stability. Besides reproducing the phases (namely, $C2/m$ Na_3B_2, $I4/mmm$ Na_2B_3, $I4/mmm$ NaB_4, and Pm Na_2B_{17}) already reported by our group at 100 GPa,[24] we have identified eight novel compounds as being stable, including Na-rich phases (*Imma* Na_9B, P-1 Na_5B, $Cmcm$ Na_2B, and $P2_1/m$ Na_3B_2) and B-rich ones ($Imm2$ Na_2B_3, *Imma* Na_2B_3, $Cmmm$ NaB_2, and $Pmm2$ NaB_7), whose stable pressure ranges are shown in Fig. 1(b). It should be noted that Na_9B becomes the

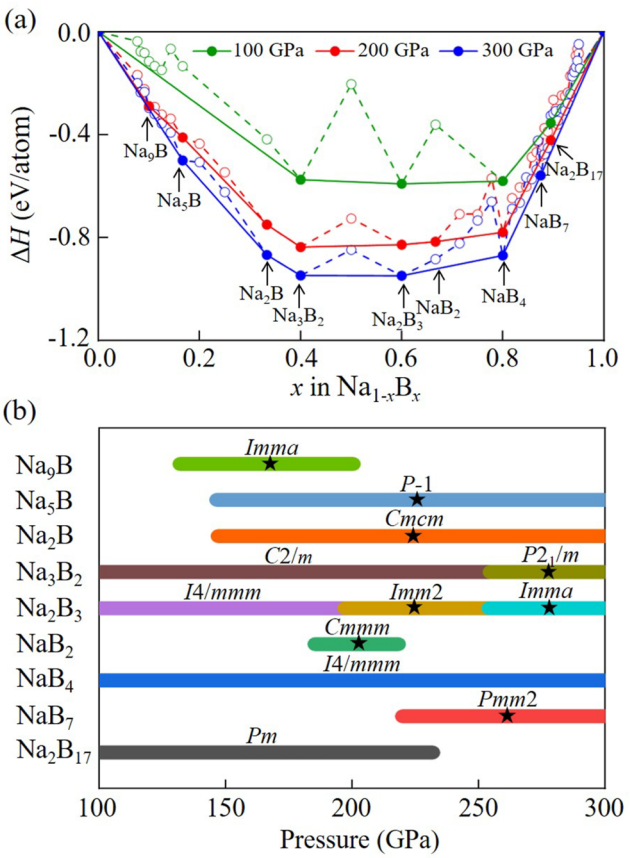

FIG. 1. (a) Convex hull of Na–B compounds at 100–300 GPa. The reference elementary structures are *fcc*, *tI*19, and *hP*4 for Na,[7] and the α-Ga phase for B,[60] adopted at the corresponding stable pressures. (b) Pressure–composition phase diagram of the Na–B system. The black stars represent the new stable phases identified in this work.

alkali-metal-richest stoichiometry among the known high-pressure alkali-metal borides. On the other hand, the absence of imaginary frequencies on the phonon dispersion curves in the whole Brillouin zone demonstrates their dynamical stability (Fig. S1, supplementary material).

To evaluate the synthetic feasibility of these newly identified compounds, we have computed their enthalpies of formation in their stable pressure regions relative to Na/B elemental solids and Na–B compounds (NaB_3, NaB_{15}, and Na_3B_{20}) stabilized at ambient pressure. As depicted in Fig. S2 (supplementary material), each predicted compound exhibits the potential for synthesis as indicated by a negative enthalpy of formation. Additionally, the optimal synthetic pathway is clearly identified with a pentagram symbol. Furthermore, it is worth noting that the precursor materials required for synthesizing each compound vary. For instance, Na and NaB_{15} serve as the starting materials for Na_9B, while Na_3B_{20} and NaB_{15} are the precursors for NaB_7.

B. Crystal structures

Despite differences in chemical composition and structural symmetry [Figs. 2(a)–2(g)], the crystal structures of stable Na–B compounds exhibit a common feature of a host–guest structure, in which host structures prefer the Na/B-rich stoichiometry [Fig. 2(h)]. This is distinguished by comparing the coordination numbers of the Na/B atoms in NaB_n/BNa_n polyhedra, in which the central atom with the lower coordination number is the host. In detail, the degree of aggregation of the building block associated with Na atoms increases with Na content, which changes from a single atom in *Pmm*2 NaB_7 to a zigzag chain in *Cmmm* NaB_2 and a wrinkled ladder chain in *Imma* Na_2B_3, to a Na_8 ring in $P2_1/m$ Na_3B_2, to a quadrangular chain and a Na_6 ring in *Cmcm* Na_2B, and eventually to a Na_{15}/Na_{16} polyhedron in *P*-1 Na_5B/*Imma* Na_9B. The same trend of variation can be found with increasing B content. On the other hand, with increasing Na content in these compounds, the amount of charge obtained by B atoms gradually increases and finally converges [i.e., the B atom has a closed-shell electronic configuration, Fig. 3(a)], as observed in Li–B compounds.[29]

Na-rich Na_9B and Na_5B are stabilized in orthorhombic [space group *Imma*, Fig. 2(a)] and triclinic [space group *P*-1, Fig. 2(b)] structures, respectively. For the Na-richest Na_9B, a three-dimensional Na lattice is formed through Na_{16} polyhedra sharing vertices and faces, in which irregular voids between these polyhedra can accommodate electrons donated by Na atoms, as will be discussed below. In Na_5B, the Na atomic motif is connected by Na_{15} polyhedra through shared vertices and edges, and the size and number of voids are also decreased compared with those of Na_9B owing to the smaller polyhedron. Furthermore, the B atoms are located at the center of the polyhedra of these two structures and are hypercoordinated (16- and 15-fold coordination for Na_9B and Na_5B, respectively). The average lengths of the Na–Na/B bonds in Na_9B at 200 GPa and Na_5B at 300 GPa are 2.21/2.31 and 2.20/2.20 Å, respectively, which are comparable to the 2.17 Å of the Na–Na bond in Na_6Au[38] and the 2.18 Å of the Li–B bond in Li_6B at 100 GPa.[29]

Cmcm Na_2B, $P2_1/m$ Na_3B_2, *Imm*2 Na_2B_3, *Imma* Na_2B_3, and *Cmmm* NaB_2 [Figs. 2(c)–2(f) and S3, supplementary material], consist of a metallic network connected by Na atoms and a covalent structure formed by B atoms (Figs. S3 and S4, supplementary material). Interestingly, *Cmcm* Na_2B [Fig. 2(c)], can be considered as a variant of the host–guest structure *tI*19-Na.[2] The host-type metallic Na network with an Na–Na distance of 1.80–2.63 Å at 200 GPa is the same as that of the *tI*19-Na phase. For the guest structure, the B atoms form a zigzag chain with a bond length of 1.55 Å, which not only places the guest position of the Na linear chain in the *tI*19-Na phase, but also inserts into the unoccupied octagonal channels, which can be attributed to the smaller radius of the B atom.

Na_3B_2 adopts a monoclinic structure with the $P2_1/m$ space group at pressures ranging from 255 to 300 GPa [Fig. 2(d)]. Specifically, Na atoms arrange themselves into a flat plane formed by edge-sharing Na_8 rings in the *ac* plane. This plane is then staggered along the *b* axis to create an interconnected network of Na atoms with helical channels. On the other hand, B atoms form a stripe-like arrangement along the *b* axis, composed of B_3 triangles that share edges and are positioned at the centers of the helical Na channels.

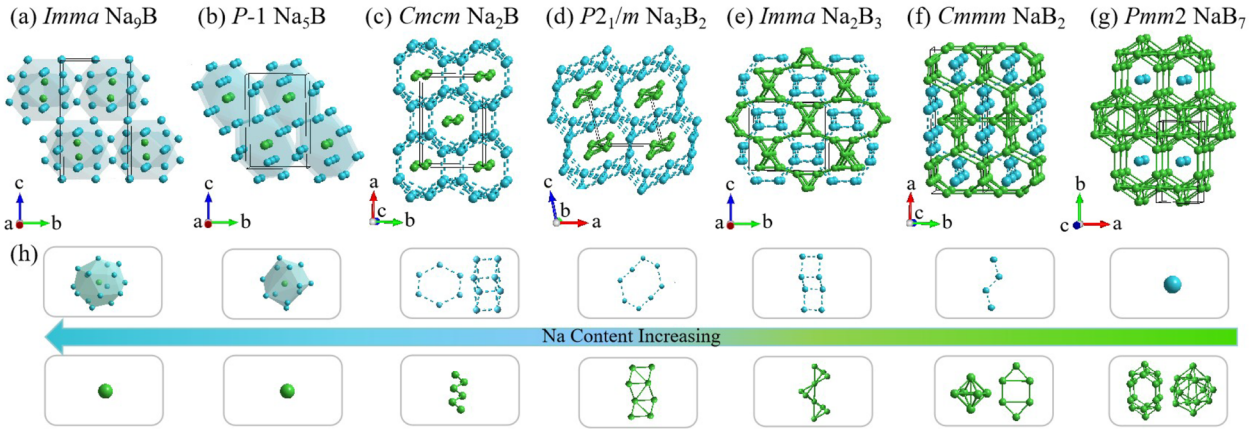

FIG. 2. Crystal structures of (a) *Imma* Na_9B at 200 GPa, (b) *P*-1 Na_5B at 300 GPa, (c) *Cmcm* Na_2B at 200 GPa, (d) $P2_1/m$ Na_3B_2 at 300 GPa, (e) *Imma* Na_2B_3 at 300 GPa, (f) *Cmmm* NaB_2 at 200 GPa, and (g) *Pmm*2 NaB_7 at 300 GPa. (h) Variations of Na/B atomic building blocks of stable compounds with Na content. Blue and green spheres represent Na and B atoms, respectively.

Considering that the *Imm*2 and *Imma* phases of Na_2B_3 belong to the orthorhombic crystalline system [Figs. 2(e) and S3, supplementary material], here we have analyzed their phase-transition process, which can be understood from the variations of Na and B units. The low-pressure *Imm*2 phase is composed of alternating Na_4 tetrahedra and Na_2 dimers via vertex-sharing. With pressure, the Na_2 dimers along the *a* axis rotate toward the *b* axis, accompanied by ruptures of the Na_4 tetrahedra, leading to the formation of a folded ladder shape. With regard to the B units, *Imm*2 Na_2B_3 consists of alternating B_4 tetrahedra and B_4 quadrilaterals (two B_3 triangles sharing edges) through shared vertices. The increased pressure results in a greater degree of folding of the B_4 quadrilaterals, and eventually they transform into B_4 tetrahedra, which can be viewed as a linear chain made up of vertex-sharing B_4 tetrahedra. Meanwhile, the decreasing distances between Na/B atoms under high pressure play an important role in making the structure more compact.

NaB_2 is predicted to adopt a *Cmmm* symmetry [Fig. 2(f)], where the B atoms form a three-dimensional framework featuring octagonal channels along the *b* axis. This framework can be understood as being composed of two building blocks: a B_6 octahedron and a B_6 hexagon. Moreover, a Na network is formed within the octagonal channels, with an Na–Na distance ranging from 1.98 to 2.17 Å at 200 GPa. The Na network is embedded within the structure, contributing to the overall stability and arrangement of the compound.

The B-richest NaB_7 stabilizes in an orthorhombic structure with *Pmm*2 symmetry [Fig. 2(g)]. There, the B atoms form a three-dimensional covalent framework composed of B_{18} hexadecahedra and B_{14} icositetrahedra through face-sharing, and each Na atom is located at the center of the B_{18} hexadecahedron. The B–B bond length is in the range of 1.54–1.74 Å at 300 GPa, which is shorter than the 1.80 Å in γ-B,[60] confirming its covalent bonding characteristics, as evidenced by the electron localization function (ELF) analysis [see Fig. 5(a)]. Furthermore, the interaction between Na and B atoms, with a bonding length of 1.96–2.48 Å, is ionic, which is in agreement with the Bader analysis [Fig. 3(a)].

C. Electronic, superionic, and superconducting properties

Diverse elemental compositions and atomic arrangements in compounds often result in varied and distinct properties.[17] In the case of our predicted compounds, their properties exhibit a dependence on B content. Specifically, as the B content increases, these compounds undergo a transformation from being semiconductors (Na_9B and Na_5B) to metals (Na_2B, Na_2B_3, and NaB_2) or superconductors (Na_3B_2 and NaB_7), as observed in the calculated electronic band structures, the projected density of states (PDOS), and the superconductivity analysis (Fig. S5 and Table S3, supplementary material). Additionally, the B-poor compound Na_9B exhibits unexpected electride and superionic features. Therefore, we discuss their properties in order of increasing B content.

For Na_9B, the electron localization function (ELF) reveals that some of the valence electrons are localized around the B atoms, and the others, known as interstitial anion electrons (IAEs), are located in the BNa_{16} polyhedral cavities in an irregular shape, showing an electride feature [Fig. 3(b)]. The Na–B bond has an ionicity, which is mainly attributed to the interaction between Na 3*s* and B $2s/2p_x/2p_z$ [Fig. 3(c)]. On the other hand, considering the local IAEs in the polyhedra, we can conclude that the nonmetallicity of Na_9B is attributable not only to the superimposed Na–B interaction caused by hypercoordination, but also to the interaction between Na cations and IAEs located in the polyhedral cavities. With pressure, Na atoms donate more electrons to interstitial regions and B atoms, and the localization of these electrons is enhanced, resulting in an increased bandgap in Na_9B [Figs. 3(d) and S6 and Table S2, supplementary material].

Pressure-induced superionicity in materials has recently attracted research interest,[35,61] especially because of the observed coexistence of electride and superionic states in Li_6Al.[20] Here, we

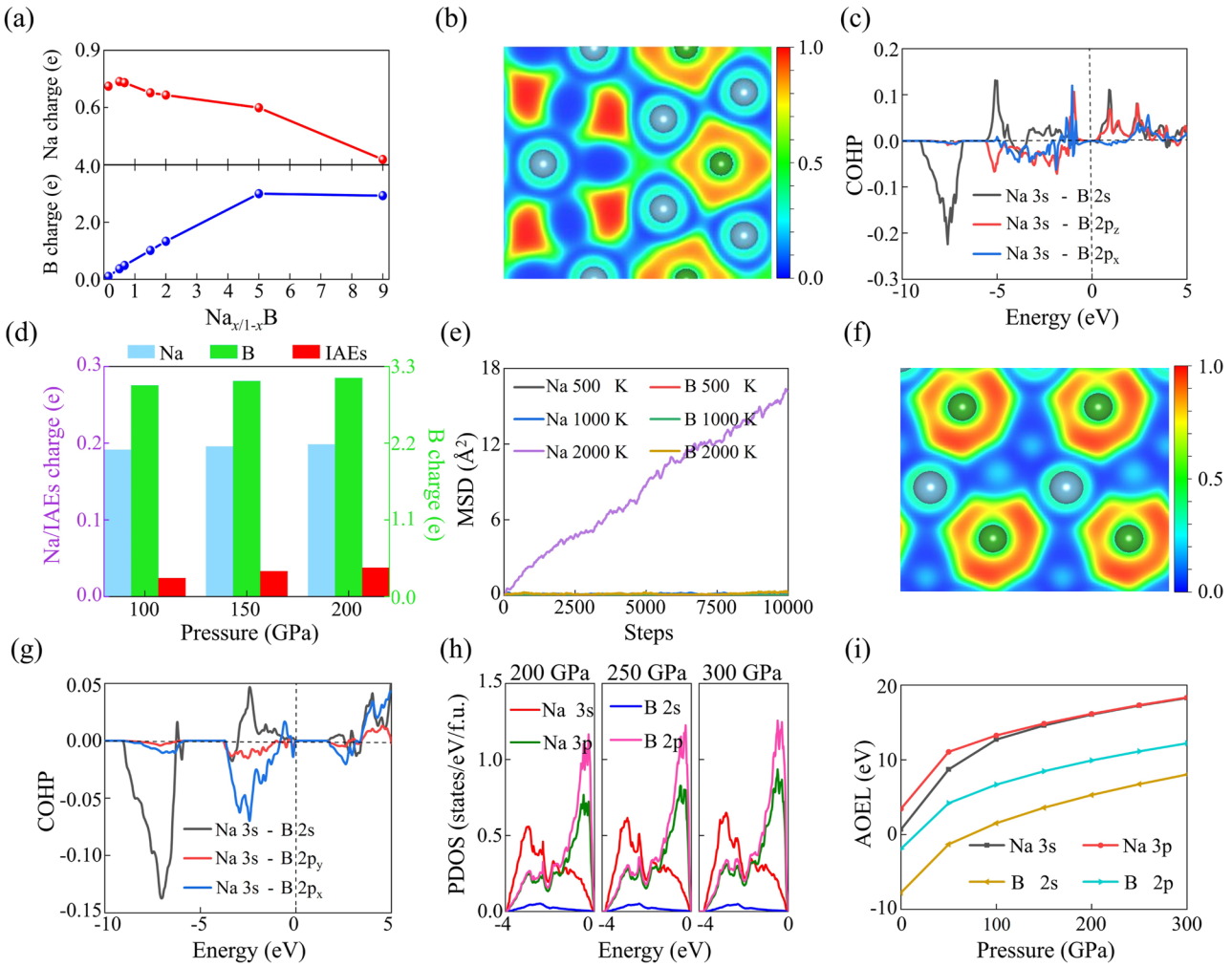

FIG. 3. (a) Amount of charge donated/accepted from the Na/B atom in stable Na–B compounds. (b) Electron localization function (ELF) in the (100) plane and (c) crystal orbital Hamilton population (COHP) of the Na–B pair with a distance of 2.30 Å (−0.32 eV/pair) in *Imma* Na_9B at 200 GPa. (d) Donated (Na)/accepted [B and interstitial anion electrons (IAEs)] charge amount in *Imma* Na_9B under different pressures. (e) Mean-squared displacement (MSD) of Na_9B at different temperatures with *NVT* conditions. (f) ELF in the (100) plane and (g) COHP of the Na–B pair with a distance of 2.25 Å (−0.36 eV/pair) in *P*-1 Na_5B at 300 GPa. (h) Projected density of states (PDOS) in the valence band region of *P*-1 Na_5B at different pressures. (i) Atomic orbital energy levels (AOELs) for Na and B atoms as functions of external pressure.

have explored the potential superionicity in the Na_9B electride via AIMD simulations. According to the MSD and the atomic trajectories, we can calculate the diffusion coefficients D and analyze the motion behaviors of Na/B atoms at 500–3000 K to determine if the superionic state appears. At 500–1250 K, $D_{Na} \approx D_B \approx 0$, indicating that Na_9B is a solid state where both Na and B atoms vibrate around their equilibrium positions (Figs. S7 and S8, supplementary material). On heating to 2000 K, the heavier Na atoms exhibit obvious diffusion ($D_{Na} = 2.6 \times 10^{-5}$ cm^2/s > 0, $D_B \approx 0$) [Fig. 3(e)], and the compound enters a superionic state, with a diffusion coefficient comparable to those of other Na-based superionic compounds.[62,63] When the temperature rises to 2850 K [Fig. S7(d), supplementary material], it begins to transform into a liquid state, while complete melting requires a higher temperature.

Among the superionic compounds studied so far, diffusion of lighter atoms is more commonly observed.[20,35,61] However, there are also some compounds that exhibit superionic behavior in heavier atoms.[64,65] It is important to highlight that the diffusion behavior of the heavier Na atoms in this work can be explained by an unusual mechanism, in which Na atomic motions are influenced by IAEs. Owing to the irregularity of the interstitial electronic morphology, the Na1 atom, located at the position where two polyhedra are connected [black dashed oval in Fig. 4(a)], is closer to the IAEs, and so it is easily attracted and deviates from its equilibrium position to position A. Meanwhile, this behavior causes the appearance of a vacancy

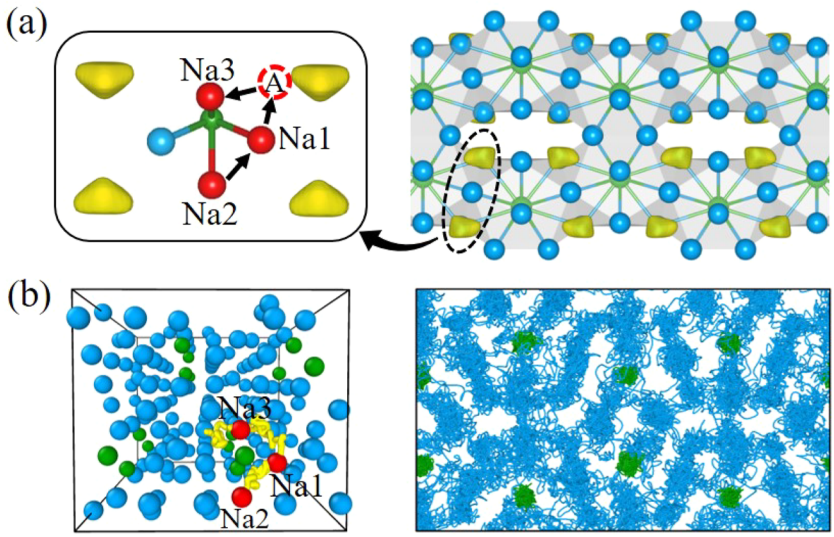

FIG. 4. (a) Schematics of the mechanism of the superionic behavior (left side), and ELF (right side) of Na_9B. (b) Early trajectories of selected Na atoms in a representative polyhedron (left side) and the late trajectories of all atoms (right side) of Na_9B at 200 GPa and 2000 K after the onset of superionicity. The blue and green spheres represent Na and B atoms, respectively, and the red spheres are the initially diffusing Na atoms.

and induces other Na atoms (e.g., Na2) to move toward it, and the Na atom at position A will also move to another equilibrium position (e.g., Na3) owing to repulsion by Na cations. This phenomenon explains the initial motion of Na atoms within a representative polyhedron. Given that the structure consists of multiple such polyhedra, numerous Na atoms within these polyhedra begin to move owing to the attraction of IAEs, resulting in the formation of multiple vacancies. Subsequently, Na atoms diffuse along various pathways within and between the polyhedra, ultimately leading to diffusion throughout the lattice [Figs. 4(b) and S9, supplementary material]. It is noteworthy that the superionic behavior in Na_9B is also influenced by the weak Na–B/Na–Na interactions. This suggests that achieving superionic behavior in the *hP*4 Na electride with strong Na–Na interactions is challenging (Table S1, supplementary material). In addition, at any given moment, only a small portion of the Na atoms in the BNa_{16} polyhedra diffuse into adjacent polyhedra, and so the B atoms are still bound.

In condensed matter physics, in addition to studying macroscopic atomic movements, it is crucial to gain a deeper understanding of temperature-dependent variations of electronic properties.[66,67] Interestingly, the electride characteristics of Na_9B persist from the solid to the liquid region, accompanied by morphological changes of the IAEs as the temperature increases (up to 3000 K) (Fig. S10, supplementary material). This behavior is similar to that observed in the *hP*4 Na electride at high temperatures.[66] In the solid region, Na_9B is a semiconductor, and its bandgap gradually decreases with increasing temperature (Figs. S8 and S11, supplementary material). However, in the superionic region, it becomes a metal, and the electronic states at the Fermi level E_F increase with temperature (Figs. S8 and S11, supplementary material). The metallic behavior is primarily attributed to the contribution of Na 3*p*/3*s* electrons, which is related to the charge transfer from 3*s* to 3*p* orbitals of Na atoms [Fig. 3(i)]. It is worth noting that the absence of an Na *d* orbital in Na_9B distinguishes it from IAEs with *d*-orbital attributes in the *hP*4 Na electride.[66]

Compared with Na_9B, Na_5B contains fewer valence electrons contributed by Na atoms and smaller polyhedral cavities, and so the valence electrons are located mainly around the boron atoms, as shown by the ELF [Fig. 3(f)]. On the other hand, the calculated crystal orbital Hamilton population (COHP) of the Na–B bond is comparable to that of Na_9B [Fig. 3(g)], which is associated with the hybridized state of Na 3*s* and B $2s/2p_x/2p_y$. Therefore, its nonmetallicity is a consequence of the superimposed ionic interaction between Na and B atoms. Furthermore, the bandgap of Na_5B gradually increases (Table S2, supplementary material), and many more electrons, especially from the B 2*p* and Na 3*p* orbitals, occupy the upper part of the valence band with pressure [Fig. 3(h)]. The former is associated with a band flattening induced by the strong electronic localization (Figs. S12 and S13, supplementary material), and the latter is attributed to the increasing amount of Na → B charge transfer (Table S2, supplementary material). The pressure-dependent variation of atomic orbital energy levels also supports the analysis above [Fig. 3(i)].

With increasing B content, compounds such as Na_2B, Na_3B_2, Na_2B_3, NaB_2, and NaB_7 exhibit metallic properties, primarily due to the contribution of the B 2*p* electrons, as indicated by the PDOS (Fig. S5). Among these compounds, the Na-rich Na_3B_2 shows superconductivity, albeit with a very low T_c of 0.01 K at 300 GPa, which can be attributed to the weak electron–phonon coupling (Table S3, supplementary material).

As far as the B-rich NaB_7 is concerned, this has a unique B cage and a high DOS at the E_F, which is promising with regard to enhanced superconductivity, and thus we focus on analyzing its electronic and superconducting properties. In the projected elec-

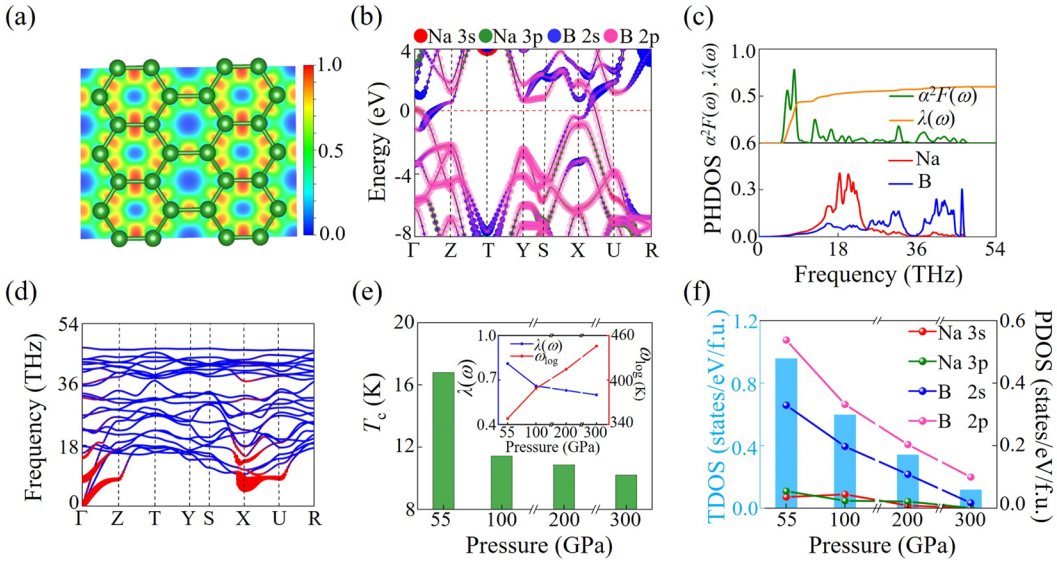

FIG. 5. (a) ELF in the (001) plane, (b) projected electronic band structure, (c) Eliashberg spectral function $\alpha^2F(\omega)$, electron–phonon coupling (EPC) parameter λ, projected phonon density of states (PHDOS), and (d) phonon dispersion curves (with the magnitude of λ indicated by the thickness of the red curves) of *Pmm*2 NaB_7 at 300 GPa. (e) Pressure-dependent T_c, λ, and ω_{log}, and (f) total and projected DOS at the E_F of *Pmm*2 NaB_7.

tronic band structure [Fig. 5(b)], there is a flat band along the Γ–Z direction and around the X point near the E_F, resulting in a Van Hove singularity with a large DOS at E_F [Fig. S5(g), supplementary material], and two steep bands cross the E_F along the X–U direction. It is worth noting that there are distinct nesting behaviors observed in the Fermi surfaces along the Γ–Z direction and around the X point, as evidenced by the pronounced peaks in the Fermi surface nesting function ξ(*Q*) (Fig. S14, supplementary material). According to Bardeen–Cooper–Schrieffer (BCS) theory,[68] this obvious "flat band–steep band" characteristic, the large DOS at the E_F, and the Fermi surface nesting behaviors imply that *Pmm*2 NaB_7 is a potential superconductor.

The calculated electron–phonon coupling (EPC) parameter λ of NaB_7 is 0.60 at 300 GPa, which is comparable to the 0.70 of MgB_2 at 0 GPa,[69] and higher than the 0.36 of *C*2/*m* ScB_6 at 500 GPa.[70] According to the Eliashberg spectral function and the projected phonon density of states (PHDOS) [Fig. 5(c)], the vibrations of Na and B atoms are obviously coupled in the whole phonon frequency range. Low-frequency vibrations below 11.3 THz contribute 73.9% of the total λ, while high-frequency vibrations contribute 26.1%. The strong EPC dominated by low frequencies can be attributed to the phonon softening along the Γ–Z direction and around the X point [Fig. 5(d)], which is associated with the flat-band feature near the E_F and the behavior of the Fermi surface nesting (Fig. S14, supplementary material). According to the Allen–Dynes-modified McMillan equation,[71] the estimated superconducting transition temperature T_c is 10.2 K at 300 GPa with the typical Coulomb pseudopotential parameter of $\mu^* = 0.1$, which is comparable to the 9.0 K of α-BeB_6 at 1 atm,[72] and higher than the 1.0 K of *Amm*2 Mg_3B_{10} at 40 GPa[73] and the 0.2 K of *Immm* SrB_8 at 150 GPa.[74]

For pressure-induced superconductivity, dynamically stabilized pressure of materials is crucial for further experimental verifications and applications. Interestingly, the dynamic stability of NaB_7 can be maintained as low as 55 GPa (Fig. S15, supplementary material), which prompts us to investigate its pressure-dependent superconductivity [Fig. 5(e) and Table S3, supplementary material]. As pressure decreases, T_c gradually increases, reaching a maximum value of 16.8 K at 55 GPa (Fig. S16, supplementary material). Since the λ and ω_{log} are the two key parameters determining the value of T_c, their variations with pressure are also analyzed. In detail, as pressure decreases, λ increases and ω_{log} decreases. Thus, λ plays a leading role in the evolution of the value of T_c. The higher value of λ at low pressure can be attributed to the increased DOS at the E_F, especially from the 2*s* and 2*p* electrons of B atoms [Fig. 5(f)].

IV. CONCLUSIONS

In summary, we have performed first-principles swarm-intelligent structure search calculations to construct the high-pressure (100–300 GPa) phase diagram of the Na–B system with various chemical compositions. Eight novel Na–B compounds (two semiconductors and six metals) have been identified as being stable. All compounds can be seen as host–guest structures, and they exhibit novel Na/B atomic building blocks regulated by the Na/B content. In particular, *Imma* Na_9B is the alkali-metal-richest boride and exhibits coexisting superionic and electride characteristics at 200 GPa and 2000 K. With increasing temperature, it also experiences a transition from a semiconductor to a metal related to Na 3*p*/3*s* states. Additionally, B-rich NaB_7, with unique B cages, has an estimated T_c of 16.8 K at 55 GPa, which is mainly due to the coupling of B 2*p* electrons and low-frequency phonons. Our work represents

an important step in furthering understanding the structures and properties of high-pressure alkali-metal borides.

SUPPLEMENTARY MATERIAL

See the supplementary material for the following: computational details, fitted Birch–Murnaghan equations of state, phonon dispersion curves, potential synthesis routes, ELFs, electronic band structures, PDOS, and structural information on stable Na–B compounds; crystal structures of *Imm*2 and *Imma* Na_2B_3; trajectories, temperature-dependent phase diagram, ELF, and PDOS of *Imma* Na_9B at 500–3000 K; several trajectories of Na atoms in other representative polyhedra of *Imma* Na_9B at 200 GPa and 2000 K; charge transfer amounts and bandgaps of *Imma* Na_9B and *P*-1 Na_5B at different pressures; the Fermi surface nesting function $\xi(Q)$ of *Pmm*2 NaB_7 at 300 GPa; the integrated COHPs (ICOHPs) of *hP*4 Na and *Imma* Na_9B at 200 GPa; and superconducting properties of the metallic Na–B phases.

ACKNOWLEDGMENTS

This work was supported by the Natural Science Foundation of China under Grant No. 21573037, the Postdoctoral Science Foundation of China under Grant No. 2013M541283, the Natural Science Foundation of Hebei Province (Grant No. B2021203030), and the Science and Technology Project of Hebei Education Department (Grant Nos. JZX2023020 and QN2023246). A.B. acknowledges financial support from the Spanish Ministry of Science and Innovation (Grant No. PID2019-105488GB-I00) and the Department of Education, Universities and Research of the Basque Government and the University of the Basque Country (Grant No. IT1707-22). This work was carried out at the National Supercomputer Center in Tianjin, and the calculations were performed on TianHe-1(A).

AUTHOR DECLARATIONS

Conflict of Interest

The authors have no conflicts to disclose.

Author Contributions

Z.G. and X.L. contributed equally to this work.

Zixuan Guo: Investigation (equal); Visualization (equal); Writing – original draft (equal). **Xing Li**: Investigation (equal); Visualization (equal); Writing – original draft (equal). **Aitor Bergara**: Writing – review & editing (supporting). **Shicong Ding**: Visualization (supporting). **Xiaohua Zhang**: Writing – review & editing (supporting). **Guochun Yang**: Resources (lead); Supervision (lead); Writing – review & editing (lead).

DATA AVAILABILITY

The data that support the findings of this study are available from the corresponding author upon reasonable request.

REFERENCES

[1] E. Wigner and F. Seitz, "On the constitution of metallic sodium," Phys. Rev. **43**, 804 (1933).
[2] B. Rousseau, Y. Xie, Y. Ma, and A. Bergara, "Exotic high pressure behavior of light alkali metals, lithium and sodium," Eur. Phys. J. B **81**, 1–14 (2011).
[3] R. J. Nelmes, M. I. McMahon, J. S. Loveday, and S. Rekhi, "Structure of Rb-III: Novel modulated stacking structures in alkali metals," Phys. Rev. Lett. **88**, 155503 (2002).
[4] H. Olijnyk and W. B. Holzapfel, "Phase transitions in K and Rb under pressure," Phys. Lett. A **99**, 381–383 (1983).
[5] Y. Ma, A. R. Oganov, and Y. Xie, "High-pressure structures of lithium, potassium, and rubidium predicted by an *ab initio* evolutionary algorithm," Phys. Rev. B **78**, 014102 (2008).
[6] G. Fabbris, J. Lim, L. S. I. Veiga, D. Haskel, and J. S. Schilling, "Electronic and structural ground state of heavy alkali metals at high pressure," Phys. Rev. B **91**, 085111 (2015).
[7] Y. Ma, M. Eremets, A. R. Oganov, Y. Xie, I. Trojan, S. Medvedev, A. O. Lyakhov, M. Valle, and V. Prakapenka, "Transparent dense sodium," Nature **458**, 182–185 (2009).
[8] T. Matsuoka and K. Shimizu, "Direct observation of a pressure-induced metal-to-semiconductor transition in lithium," Nature **458**, 186–189 (2009).
[9] M. Marqués, M. I. McMahon, E. Gregoryanz, M. Hanfland, C. L. Guillaume, C. J. Pickard, G. J. Ackland, and R. J. Nelmes, "Crystal structures of dense lithium: A metal-semiconductor-metal transition," Phys. Rev. Lett. **106**, 095502 (2011).
[10] H. Hosono, S.-W. Kim, S. Matsuishi, S. Tanaka, A. Miyake, T. Kagayama, and K. Shimizu, "Superconductivity in room-temperature stable electride and high-pressure phases of alkali metals," Philos. Trans. R. Soc., A **373**, 20140450 (2015).
[11] Y. Sun, L. Zhao, C. J. Pickard, R. J. Hemley, Y. Zheng, and M. Miao, "Chemical interactions that govern the structures of metals," Proc. Natl. Acad. Sci. U. S. A. **120**, e2218405120 (2023).
[12] Y. Li, Y. Wang, C. J. Pickard, R. J. Needs, Y. Wang, and Y. Ma, "Metallic icosahedron phase of sodium at terapascal pressures," Phys. Rev. Lett. **114**, 125501 (2015).
[13] P. S. Krstic, J. P. Allain, F. J. Dominguez-Gutierrez, and F. Bedoya, "Unraveling the surface chemistry processes in lithiated and boronized plasma material interfaces under extreme conditions," Matter Radiat. Extremes **3**, 165–187 (2018).
[14] A. Rodriguez-Prieto, A. Bergara, V. M. Silkin, and P. M. Echenique, "Complexity and Fermi surface deformation in compressed lithium," Phys. Rev. B **74**, 172104 (2006).
[15] A. Bergara, J. B. Neaton, and N. W. Ashcroft, "Pairing, π-bonding, and the role of nonlocality in a dense lithium monolayer," Phys. Rev. B **62**, 8494 (2000).
[16] A. Rodriguez-Prieto and A. Bergara, "Pressure induced complexity in a lithium monolayer: *Ab initio* calculations," Phys. Rev. B **72**, 125406 (2005).
[17] X. Li, X. Zhang, A. Bergara, Y. Liu, and G. Yang, "Structural and electronic properties of Na-B-H compounds at high pressure," Phys. Rev. B **106**, 174104 (2022).
[18] Y. Sun, J. Lv, Y. Xie, H. Liu, and Y. Ma, "Route to a superconducting phase above room temperature in electron-doped hydride compounds under high pressure," Phys. Rev. Lett. **123**, 097001 (2019).
[19] X. Dong, A. R. Oganov, A. F. Goncharov, E. Stavrou, S. Lobanov, G. Saleh, G.-R. Qian, Q. Zhu, C. Gatti, V. L. Deringer, R. Dronskowski, X. F. Zhou, V. B. Prakapenka, Z. Konôpková, I. A. Popov, A. I. Boldyrev, and H. T. Wang, "A stable compound of helium and sodium at high pressure," Nat. Chem. **9**, 440–445 (2017).
[20] X. Wang, Y. Wang, J. Wang, S. Pan, Q. Lu, H.-T. Wang, D. Xing, and J. Sun, "Pressure stabilized lithium-aluminum compounds with both superconducting and superionic behaviors," Phys. Rev. Lett. **129**, 246403 (2022).
[21] P. Baettig and E. Zurek, "Pressure-stabilized sodium polyhydrides: NaH_n ($n > 1$)," Phys. Rev. Lett. **106**, 237002 (2011).
[22] H.-K. Mao, B. Chen, J. Chen, K. Li, J.-F. Lin, W. Yang, and H. Zheng, "Recent advances in high-pressure science and technology," Matter Radiat. Extremes **1**, 59–75 (2016).
[23] A. Hermann, A. Suarez-Alcubilla, I. G. Gurtubay, L.-M. Yang, A. Bergara, N. W. Ashcroft, and R. Hoffmann, "LiB and its boron-deficient variants under pressure," Phys. Rev. B **86**, 144110 (2012).

[24]S. Zhang, X. Du, J. Lin, A. Bergara, X. Chen, X. Liu, X. Zhang, and G. Yang, "Superconducting boron allotropes," Phys. Rev. B **101**, 174507 (2020).
[25]T. Chen, Q. Gu, Q. Chen, X. Wang, C. J. Pickard, R. J. Needs, D. Xing, and J. Sun, "Prediction of quasi-one-dimensional superconductivity in metastable two-dimensional boron," Phys. Rev. B **101**, 054518 (2020).
[26]P. Zhang, Y. Tian, Y. Yang, H. Liu, and G. Liu, "Stable Rb-B compounds under high pressure," Phys. Rev. Res. **5**, 013130 (2023).
[27]X.-L. He, X. Dong, Q. Wu, Z. Zhao, Q. Zhu, A. R. Oganov, Y. Tian, D. Yu, X.-F. Zhou, and H.-T. Wang, "Predicting the ground-state structure of sodium boride," Phys. Rev. B **97**, 100102 (2018).
[28]B. Zhao, X. Wang, L. Yu, Y. Liu, X. Chen, B. Yang, G. Yang, S. Zhang, L. Gu, and X. Liu, "Fabrication of alkali metal boride: Honeycomb-like structured NaB_4 with high hardness and excellent electrical conductivity," Adv. Funct. Mater. **32**, 2110872 (2022).
[29]F. Peng, M. Miao, H. Wang, Q. Li, and Y. Ma, "Predicted lithium-boron compounds under high pressure," J. Am. Chem. Soc. **134**, 18599–18605 (2012).
[30]K. Jun, Y. Sun, Y. Xiao, Y. Zeng, R. Kim, H. Kim, L. J. Miara, D. Im, Y. Wang, and G. Ceder, "Lithium superionic conductors with corner-sharing frameworks," Nat. Mater. **21**, 924–931 (2022).
[31]M. Hara, M. Kitano, and H. Hosono, "Ru-loaded C12A7:(e^-) electride as a catalyst for ammonia synthesis," ACS Catal. **7**, 2313–2324 (2017).
[32]Y. Lu, J. Li, T. Tada, Y. Toda, S. Ueda, T. Yokoyama, M. Kitano, and H. Hosono, "Water durable electride Y_5Si_3: Electronic structure and catalytic activity for ammonia synthesis," J. Am. Chem. Soc. **138**, 3970–3973 (2016).
[33]Z. Zhao, S. Zhang, T. Yu, H. Xu, A. Bergara, and G. Yang, "Predicted pressure-induced superconducting transition in electride Li_6P," Phys. Rev. Lett. **122**, 097002 (2019).
[34]Z. Liu, Q. Zhuang, F. Tian, D. Duan, H. Song, Z. Zhang, F. Li, H. Li, D. Li, and T. Cui, "Proposed superconducting electride Li_6C by *sp*-hybridized cage states at moderate pressures," Phys. Rev. Lett. **127**, 157002 (2021).
[35]Z. Wan, W. Xu, T. Yang, and R. Zhang, "As-Li electrides under high pressure: Superconductivity, plastic, and superionic states," Phys. Rev. B **106**, L060506 (2022).
[36]Y. Wang, J. Wang, A. Hermann, C. Liu, H. Gao, E. Tosatti, H.-T. Wang, D. Xing, and J. Sun, "Electronically driven 1D cooperative diffusion in a simple cubic crystal," Phys. Rev. X **11**, 011006 (2021).
[37]H.-J. Sung, W. H. Han, I.-H. Lee, and K. J. Chang, "Superconducting open-framework allotrope of silicon at ambient pressure," Phys. Rev. Lett. **120**, 157001 (2018).
[38]X. Du, H. Lou, J. Wang, and G. Yang, "Pressure-induced Na–Au compounds with novel structural units and unique charge transfer," Phys. Chem. Chem. Phys. **23**, 6455–6461 (2021).
[39]Y. Wang, J. Lv, L. Zhu, and Y. Ma, "Crystal structure prediction via particle-swarm optimization," Phys. Rev. B **82**, 094116 (2010).
[40]Y. Wang, J. Lv, L. Zhu, and Y. Ma, "CALYPSO: A method for crystal structure prediction," Comput. Phys. Commun. **183**, 2063–2070 (2012).
[41]X. Li, X. Zhang, Y. Liu, and G. Yang, "Bonding-unsaturation-dependent superconductivity in P-rich sulfides," Matter Radiat. Extremes **7**, 048402 (2022)..
[42]D. Duan, Y. Liu, F. Tian, D. Li, X. Huang, Z. Zhao, H. Yu, B. Liu, W. Tian, and T. Cui, "Pressure-induced metallization of dense $(H_2S)_2H_2$ with high-T_c superconductivity," Sci. Rep. **4**, 6968 (2014).
[43]F. Peng, Y. Sun, C. J. Pickard, R. J. Needs, Q. Wu, and Y. Ma, "Hydrogen clathrate structures in rare earth hydrides at high pressures: Possible route to room-temperature superconductivity," Phys. Rev. Lett. **119**, 107001 (2017).
[44]H. Liu, I. I. Naumov, R. Hoffmann, N. W. Ashcroft, and R. J. Hemley, "Potential high-T_c superconducting lanthanum and yttrium hydrides at high pressure," Proc. Natl. Acad. Sci. U. S. A. **114**, 6990–6995 (2017).
[45]A. P. Drozdov, M. I. Eremets, I. A. Troyan, V. Ksenofontov, and S. I. Shylin, "Conventional superconductivity at 203 kelvin at high pressures in the sulfur hydride system," Nature **525**, 73–76 (2015).
[46]A. P. Drozdov, P. P. Kong, V. S. Minkov, S. P. Besedin, M. A. Kuzovnikov, S. Mozaffari, L. Balicas, F. F. Balakirev, D. E. Graf, V. B. Prakapenka, E. Greenberg, D. A. Knyazev, M. Tkacz, and M. I. Eremets, "Superconductivity at 250 K in lanthanum hydride under high pressures," Nature **569**, 528–531 (2019).
[47]M. Somayazulu, M. Ahart, A. K. Mishra, Z. M. Geballe, M. Baldini, Y. Meng, V. V. Struzhkin, and R. J. Hemley, "Evidence for superconductivity above 260 K in lanthanum superhydride at megabar pressures," Phys. Rev. Lett. **122**, 027001 (2019).
[48]L. Ma, K. Wang, Y. Xie, X. Yang, Y. Wang, M. Zhou, H. Liu, X. Yu, Y. Zhao, H. Wang, G. Liu, and Y. Ma, "High-temperature superconducting phase in clathrate calcium hydride CaH_6 up to 215 K at a pressure of 172 GPa," Phys. Rev. Lett. **128**, 167001 (2022).
[49]Z. Li, X. He, C. Zhang, X. Wang, S. Zhang, Y. Jia, S. Feng, K. Lu, J. Zhao, J. Zhang, B. Min, Y. Long, R. Yu, L. Wang, M. Ye, Z. Zhang, V. Prakapenka, S. Chariton, P. A. Ginsberg, J. Bass, S. Yuan, H. Liu, and C. Jin, "Superconductivity above 200 K discovered in superhydrides of calcium," Nat. Commun. **13**, 2863 (2022).
[50]G. Kresse and J. Furthmüller, "Efficient iterative schemes for *ab initio* total-energy calculations using a plane-wave basis set," Phys. Rev. B **54**, 11169 (1996).
[51]P. E. Blöchl, "Projector augmented-wave method," Phys. Rev. B **50**, 17953 (1994).
[52]J. P. Perdew, K. Burke, and M. Ernzerhof, "Generalized gradient approximation made simple," Phys. Rev. Lett. **77**, 3865 (1996).
[53]P. Blaha, K. Schwarz, P. Sorantin, and S. B. Trickey, "Full-potential, linearized augmented plane wave programs for crystalline systems," Comput. Phys. Commun. **59**, 399–415 (1990).
[54]H. J. Monkhorst and J. D. Pack, "Special points for Brillouin-zone integrations," Phys. Rev. B **13**, 5188 (1976).
[55]A. Togo, F. Oba, and I. Tanaka, "First-principles calculations of the ferroelastic transition between rutile-type and $CaCl_2$-type SiO_2 at high pressures," Phys. Rev. B **78**, 134106 (2008).
[56]S. Baroni, S. De Gironcoli, A. Dal Corso, and P. Giannozzi, "Phonons and related crystal properties from density-functional perturbation theory," Rev. Mod. Phys. **73**, 515 (2001).
[57]P. Giannozzi, S. Baroni, N. Bonini, M. Calandra, R. Car, C. Cavazzoni, D. Ceresoli, G. L. Chiarotti, M. Cococcioni, I. Dabo, A. Dal Corso, S. de Gironcoli, S. Fabris, G. Fratesi, R. Gebauer, U. Gerstmann, C. Gougoussis, A. Kokalj, M. Lazzeri, L. Martin-Samos, N. Marzari, F. Mauri, R. Mazzarello, S. Paolini, A. Pasquarello, L. Paulatto, C. Sbraccia, S. Scandolo, G. Sclauzero, A. P. Seitsonen, A. Smogunov, P. Umari, and R. M. Wentzcovitch, "QUANTUM ESPRESSO: A modular and open-source software project for quantum simulations of materials," J. Phys.: Condens. Matter **21**, 395502 (2009).
[58]D. J. Evans and B. L. Holian, "The Nose–Hoover thermostat," J. Chem. Phys. **83**, 4069–4074 (1985).
[59]X. Zhong, Y. Sun, T. Iitaka, M. Xu, H. Liu, R. J. Hemley, C. Chen, and Y. Ma, "Prediction of above-room-temperature superconductivity in lanthanide/actinide extreme superhydrides," J. Am. Chem. Soc. **144**, 13394–13400 (2022).
[60]A. R. Oganov, J. Chen, C. Gatti, Y. Ma, Y. Ma, C. W. Glass, Z. Liu, T. Yu, O. O. Kurakevych, and V. L. Solozhenko, "Ionic high-pressure form of elemental boron," Nature **457**, 863–867 (2009).
[61]C. Liu, H. Gao, A. Hermann, Y. Wang, M. Miao, C. J. Pickard, R. J. Needs, H.-T. Wang, D. Xing, and J. Sun, "Plastic and superionic helium ammonia compounds under high pressure and high temperature," Phys. Rev. X **10**, 021007 (2020).
[62]Q. Zhang, C. Zhang, Z. D. Hood, M. Chi, C. Liang, N. H. Jalarvo, M. Yu, and H. Wang, "Abnormally low activation energy in cubic Na_3SbS_4 superionic conductors," Chem. Mater. **32**, 2264–2271 (2020).
[63]Q. Chen, N. H. Jalarvo, and W. Lai, "Na ion dynamics in P2-$Na_x[Ni_{1/3}Ti_{2/3}]O_2$: A combination of quasi-elastic neutron scattering and first-principles molecular dynamics study," J. Mater. Chem. A **8**, 25290–25297 (2020).
[64]J. Li, Y. Geng, Z. Xu, P. Zhang, G. Garbarino, M. Miao, Q. Hu, and X. Wang, "Mechanochemistry and the evolution of ionic bonds in dense silver iodide," JACS Au **3**, 402–408 (2023).
[65]Y.-H. Yin and L. Zhang, "The structures and properties of $(AgCl)_n$ (n = 2–13)," Comput. Theor. Chem. **1097**, 70–78 (2016).
[66]R. Paul, S. X. Hu, V. V. Karasiev, S. A. Bonev, and D. N. Polsin, "Thermal effects on the electronic properties of sodium electride under high pressures," Phys. Rev. B **102**, 094103 (2020).

[67]D. N. Polsin, A. Lazicki, X. Gong, S. J. Burns, F. Coppari, L. E. Hansen, B. J. Henderson, M. F. Huff, M. I. McMahon, M. Millot, R. Paul, R. F. Smith, J. H. Eggert, G. W. Collins, and J. R. Rygg, "Structural complexity in ramp-compressed sodium to 480 GPa," Nat. Commun. **13**, 2534 (2022).
[68]J. Bardeen, L. N. Cooper, and J. R. Schrieffer, "Theory of superconductivity," Phys. Rev. **108**, 1175 (1957).
[69]J. Kortus, I. I. Mazin, K. D. Belashchenko, V. P. Antropov, and L. L. Boyer, "Superconductivity of metallic boron in MgB_2," Phys. Rev. Lett. **86**, 4656 (2001).
[70]J. Du, X. Li, and F. Peng, "Pressure-induced evolution of structures and promising superconductivity of ScB_6," Phys. Chem. Chem. Phys. **24**, 10079–10084 (2022).
[71]P. B. Allen and R. C. Dynes, "Transition temperature of strong-coupled superconductors reanalyzed," Phys. Rev. B **12**, 905 (1975).
[72]L. Wu, B. Wan, H. Liu, H. Gou, Y. Yao, Z. Li, J. Zhang, F. Gao, and H.-k. Mao, "Coexistence of superconductivity and superhardness in beryllium hexaboride driven by inherent multicenter bonding," J. Phys. Chem. Lett. **7**, 4898–4904 (2016).
[73]M. M. Davari Esfahani, Q. Zhu, H. Dong, A. R. Oganov, S. Wang, M. S. Rakitin, and X.-F. Zhou, "Novel magnesium borides and their superconductivity," Phys. Chem. Chem. Phys. **19**, 14486–14494 (2017).
[74]Z. Cui, Q. Yang, X. Qu, X. Zhang, Y. Liu, and G. Yang, "A superconducting boron allotrope featuring anticlinal pentapyramids," J. Mater. Chem. C **10**, 672–679 (2022).